YTUP

Journal of Thermal Engineering

https://jten.yildiz.edu.tr/

https://doi.org/10.47481/jten.0049

RESEARCH ARTICLE

Numerical investigation of flow and heat transfer characteristics of different multiple impinging jets diffusers

A.M. Maiga[1], A. Khelil[2,*], M. Braikia[3], A. Fellague Chebra[4],

[1]Hassiba BenboualiB,University of Chlef, LCTMMS Chlef, Algeria, 02000
[2]Hassiba BenboualiB,University of Chlef, LCTMMS Chlef, Algeria, 02000
[3]Hassiba BenboualiB,University of Chlef, LCTMMS Chlef, Algeria, 02000
[4]Hassiba BenboualiB,University of Chlef, LCTMMS Chlef, Algeria, 02000

Abstract

Efficient cooling of heated surfaces is crucial in many industrial applications, where improving heat transfer and air distribution plays a key role. The effect of change in geometric arrangement of a diffusion system on the cooling of a hot plate is studied. The work presents a unique comparative analysis of numerous diffuser designs. A three-dimensional simulation using the SST k-ω turbulence model was conducted on twenty-five diffusers, where the height H is defined as twice the diffuser diameter (H = 2D), and the Reynolds number is 11,600. Results show that diffuser geometry has a significant effect on air distribution and thermal efficiency. The lobed diffuser provides the highest outlet velocities which improve jet acceleration and mixing, resulting in a 31.7% increase in thermal transfer over the circular diffuser. The swirling diffuser is less effective in velocities but improves the flow uniformity, resulting in an increase of 16.26% in thermal transfer. The circular diffuser is stable but has poor heat transfer performance. In general, the lobed diffuser has the best balance between flow acceleration and thermal efficiency.

Keywords: Circular diffuser, lobed diffuser swirl, diffuser multiple, impinging jets, heat transfer, k-ω SST turbulence model

Cite this article as: Maiga, A. M., Khelil, A., Braikia, M., & Fellague Chebra, A. (2026). Numerical investigation of flow and heat transfer characteristics of different multiple impinging jets diffusers. Journal of Thermal Engineering, 12(4), 1558–1572. https://doi.org/10.47481/jten.0049

1. Introduction

The transport of heat is a very important problem in many industrial applications and has motivated a continuous quest for effective thermal management techniques. Of them, jet impingement has been shown as a very successful approach and has been extensively used in current systems for heating, cooling and food processing [1-3]. Impact jets have undergone much study throughout the years. They are categorized into three sections: free jet, stagnation, and wall jet [4]. The research initially is mostly focused on single impinging jet (SIJ) configurations, especially in the stagnation area where the heat transmission is the most intensive. But SIJs have a great disadvantage their effectiveness decreases quickly beyond the stagnation zone, which leads to an uneven temperature distribution. To circumvent this constraint, multiple impinging jets (MIJ) have been studied since they may give a more consistent heat transmission across vast areas. Industrial applications such as combustion chamber cooling, gas turbine blade thermal load management, and steel and glass quenching need appropriate MIJ setups [5-7]. Thermal and fluid dynamic characteristics of MIJ systems are dependent on the diffuser shape, jet spacing, turbulence intensity, separation distance and flow confinement [8]. Many works have studied MIJ performance for various setups. The complicated flow interactions in MIJ systems and the influence of jet-to-jet interference on the heat transfer characteristics were addressed by Geers et al. [9] and Weigand and Spring [10]. Giorges et al. [11] shown that MIJ layouts greatly enhance turbulent mixing compared to SIJs. The influence of the location and spacing of diffusers to improve the heat transfer efficiency was studied by Braikia et al. [12]. Further studies by Roudane et al. and Bennia et al. [13-14] indicated the need for turbulence modeling to predict the behavior of MIJ. Furthermore, Aziz et al. [15] examined

*Corresponding Author
E-mail Adress: a.khelil@uni-chle.dz

Submitted: 13 January 2025; **Accepted:** 10 April 2025

This paper was recommended for publication in revised form by Editor-in-Chief Ahmet Selim Dalkılıç

experimentally and computationally the airflow properties of swirl, circular and square ceiling diffusers and their influence on thermal comfort in ventilated rooms. The research showed that the velocity decay coefficient for square and circular diffusers was about the same but was 2.6 times larger for the swirl diffuser. A numerical analysis was carried out by Meslem et al. [16] to explore three different turbulence models (standard k-ε, SST k-ω, and RSM). When it comes to predicting jet interactions, dynamic expansion, and ambient air entrainment in lobe diffuser systems, the SST k-ω turbulence model has shown to be quite effective. Suzuki et al. [17] evaluated two configurations of 13 and 19 circular diffusers using DNS resolution and confirmed that the presence of many jets improves the heat transmission in the whole region, even with the crossflow effects. Some recent numerical studies have looked at different diffuser designs and jet layouts to maximize MIJ heat transmission. Debnath et al. [8] studied two circular grid arrangements, aligned and staggered, with 25 circular diffusers of 40 mm diameter each. They utilized the SST k-omega turbulence model to explore the influence of swirling flow for two distinct values of the swirl number: S = 0 and S = 0.74. Both values were used to get the results. The staggered configuration was determined to facilitate effective mixing and improve heat transmission. The peak augmentation in heat transmission happening at the stagnation point and between neighboring jets. In the direction of azimuthal motion (W), swirling jets have a velocity component that generates a rotating flow, which is represented by a swirl number (S). The precise formulation of swirl number depends on diffuser design and flow profile. The swirl number for a vane swirl diffuser is given by (Gupta et al. [18]):

$$S = \frac{\int_0^R r^2 UW\,dr}{R\int_0^R r\left(U^2 - \frac{W^2}{2}\right)dr} \quad (1)$$

Where:

r: Radial coordinate (dimensional cylindrical coordinates)

R: The maximum radius of the flow

U: Dimensionless velocity in the axial direction

W: Dimensionless velocity in the tangential direction

Another empirical expression is used to calculate the swirl number, based on the geometric characteristics of the swirl generator (according to [19]).

$$S = \frac{2}{3}\left[\frac{1 - \left(\frac{R_h}{R_n}\right)^3}{1 - \left(\frac{R_h}{R_n}\right)^2}\right] \cdot \mathrm{tg}\alpha \quad (2)$$

With:

α : The angle of the fins created a swirl generator;

R_h : The support radius of the vane diffuser;

R_n : The diffuser radius.

In addition, Vamsi et al. [20] conducted an examination of fluid dynamics and heat transport in inline circular jets by both experimental and computational methods. To improve heat transfer and air dispersion in MIJ configurations, Reynolds number, nozzle-to-plate distance, and jet spacing have all been shown to be critical factors to consider. Despite these improvements, systematic assessment of alternative diffuser designs and their influence on MIJ performance is an open research field. The present work intends to fill this gap by doing a comparative examination of different diffuser geometries and their impact on jet interactions and thermal behavior. Specifically, we will compare two grid configurations: circular and square; each of them having twenty-five circular diffusers arranged at H = 2D (D being the diffuser diameter) from the target surface, with an inter-jet spacing of S = 2D. Furthermore, three varieties of diffusers, namely circular, lobed and swirling will be investigated under the same circumstances. In contrast to other studies, the present work presents a systematic quantification of the influence of diffuser-induced flow alterations on the MIJ heat transfer efficiency using the SST k-ω turbulence model, which has been validated in forecasting complicated jet interactions [21-23]. Furthermore, the symmetry of the geometry will be used to lower the computational domain and therefore the simulation time while keeping the accuracy. The originality of this study is an in-depth examination of diffuser shape and thermal performance of MIJ. In contrast to the typical studies mainly focusing on jet spacing and turbulence modeling, our study offers a complete parametric assessment of the effects of various kinds of diffusers on flow features and heat transfer efficiency. This study's findings will be valuable for improving multiple impinging jet (MIJ) cooling processes in a variety of industrial fields, particularly in the cooling of electronic components and in the food processing industry, thus resulting in increased energy efficiency and improved thermal management strategies.

2. Materials and methods

Computational Fluid Dynamics (CFD) has been extensively accepted as a tool to analyze the flow features in several research areas [24-29]. It is an important tool for optimizing the design of air distribution systems. In computational fluid dynamics, Fluent was utilized using the commercial product ANSYS [30]. To accomplish this goal, the SST k-omega turbulence model is used for the purpose of simulating the system.

2. 1. Geometry and computational domain

This study aims to investigate which type of multiple diffuser configuration provides the best air and heat distribution. It will be conducted in two phases: the first focusing on the selection of the blowing configuration shape, and the second on determining the optimal diffuser. In the first phase, we aim to investigate an effect

that occurs when the form of an arrangement is altered of 25 diffusers positioned at a height of H = 2D from the impact surface and a separation distance of S = 2D between the centers of two diffusers, where D is the diffuser diameter. For this purpose, the diffusers will be arranged in two shapes: the first being circular and the second square, as illustrated in figure 1. To optimize heat transfer and velocity distribution, and after validating the diffuser arrangement shape, we will focus on determining the diffuser type that achieves a certain optimum, as may be seen in figure 2. In this case, we will investigate which of the three diffuser types (circular, lobed, and swirling) is most suitable.

For this study, we assume that the radial component is aligned with the y direction.

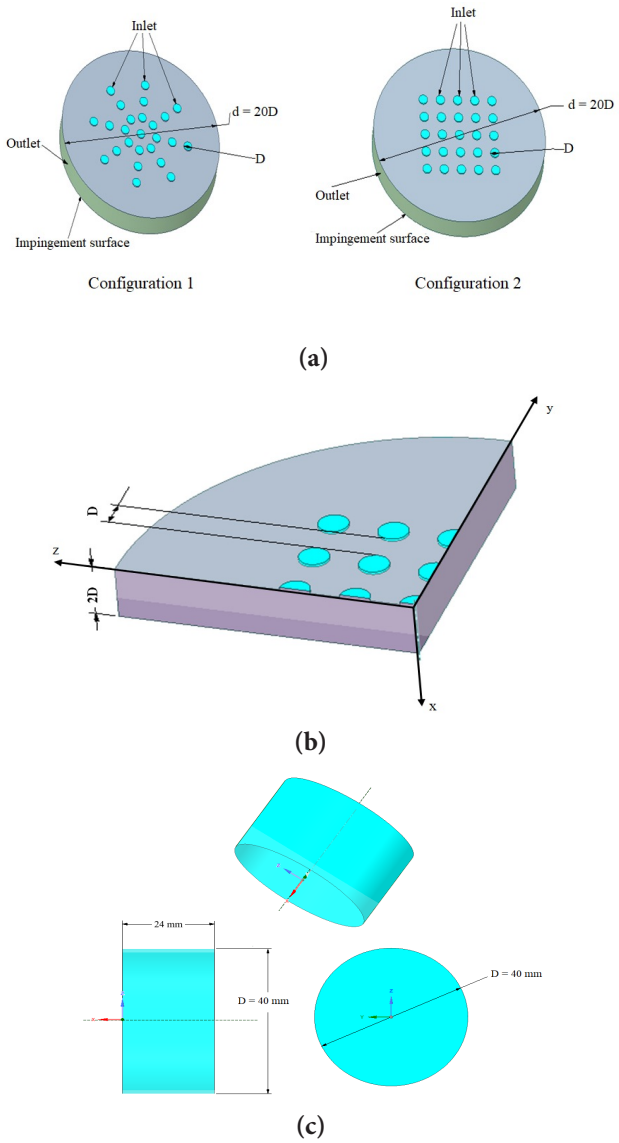

Figure 1. A schematic of the physical system: **(a)** two configurations, **(b)** quarter of configuration 2, **(c)** geometric characteristics of circular diffuser

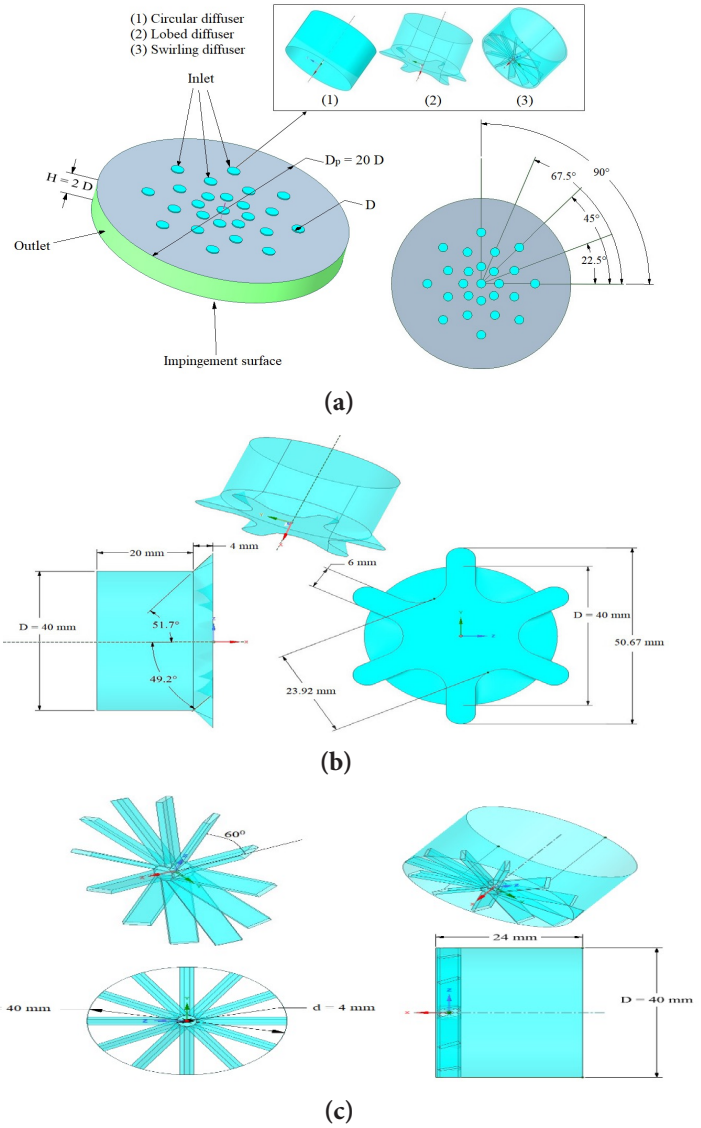

Figure 2. Problem representation with geometric characteristics: **(a)** domain of study, **(b)** geometric characteristics of lobed diffuser, **(c)** geometric characteristics of swirling diffuser

2.2. Governing equations

Within the scope of this study, we take into consideration a fluid that is incompressible and a flow that is statistically stable. The differential form and tensor notation are used to represent the continuity and momentum (RANS) equations, as shown in [31-33]:

Continuity equation

$$\frac{\partial U_i}{\partial x_i} = 0 \tag{3}$$

Momentum equation

$$\rho \frac{\partial (U_i U_j)}{\partial x_j} = -\frac{\partial P}{\partial x_i} + \frac{\partial}{\partial x_j}\left[\mu\left(\frac{\partial U_i}{\partial x_j} + \frac{\partial U_j}{\partial x_i}\right) - \rho\overline{\mu_i}'\mu_j'\right] \tag{4}$$

Energy Equation

$$\rho C_p U_i \frac{\partial T}{\partial x_i} = \frac{\partial}{\partial x_i}\left[\lambda \frac{\partial T}{\partial x_i} - \rho C_p \overline{u_i' T'}\right] \quad (5)$$

Where P and C_p are the pressure and the specific heat capacity, respectively.

u_i', u_j' and T' are the velocity and temperature fluctuations, respectively.

$-\rho\overline{u_i' u_j'}$ and $-\rho\overline{u_i' u_j'}$ are the heat fluxes and Reynolds stresses in turbulent flows, which requires explicit modeling to satisfy the governing equation system closure. [34-37].

The Boussinesq eddy-viscosity hypothesis is used in this work to create the SST k–ω model. According to the reference [38], this theory provides an explanation for the Reynolds stresses by describing them as a function of the turbulence quantities.

$$-\rho\overline{\mu_i' \mu_j'} = \mu_t\left(\frac{\partial U_i}{\partial x_j} + \frac{\partial U_j}{\partial x_i}\right) - \frac{2}{3}\left(\rho k + \mu_t \frac{\partial U_l}{\partial x_l}\right)\delta_{ij} \quad (6)$$

The variable k represents the turbulent kinetic energy, whereas the strain rate tensor is denoted by δ_{ij}. When the Boussinesq approximation is used, which assumes that the heat flow is proportional to the turbulent eddy viscosity, it is feasible to provide a description of the turbulent heat fluxes as [39].

$$-\rho\overline{u_i' T'} = \frac{\mu_t}{Pr_t}\frac{\partial T}{\partial x_i} \quad (7)$$

Here, Prt represents the turbulent Prandtl number, which is a feature of turbulent flow that acts as a metric for determining the effectiveness of turbulence mixing. In the context of this investigation, Prt equals 0.85.

In the SST k–ω turbulence model, which was created by Menter [40], the benefits of the original k–ε model are combined with those of the k–ω standard model. Because it provides a realistic depiction of flow mechanics and is numerically stable, it is used by many people. One possible way to represent the model is as follows [41-45].

$$\frac{\partial \rho U_j k}{\partial x_j} = \frac{\partial}{\partial x_j}\left[(\mu + \sigma_k \mu_t)\frac{\partial k}{\partial x_j}\right] + P_k - \beta^* \rho \omega k \quad (8)$$

$$\frac{\partial \rho U_j \omega}{\partial x_j} = \frac{\partial}{\partial x_j}\left[(\mu + \sigma_\omega \mu_t)\frac{\partial \omega}{\partial x_j}\right] + P_\omega - \beta\rho\omega^2 + 2(1 - f_1)\frac{\rho\sigma_{\omega 2}}{\omega}\frac{\partial k}{\partial x_j} \quad (9)$$

Where

The turbulent dissipation rate is denoted by ω, whereas the production terms for variables k and ω are denoted by Pk and Pω. The dissipation coefficients are β for ω and for the SST model. The diffusion coefficients for k and ω are σ_k and σ_ω, respectively.

The production terms P_k and P_ω may be written as follows:

$$P_k = \mu_t \Omega^2 \text{ and } P_\omega = C_\omega \rho \Omega^2 \quad (10)$$

Where Ω is the vorticity magnitude. The μ_t is defined as:

$$\mu_t = \frac{a_1 k}{\max(a_1 \omega, f_2 \|\Omega\|)} \quad (11)$$

In this equation, a1 stands for the experimental constant, which has a value of 0.31, and f2 is the mixing function, which is represented by equation (12):

$$f_2 = \tanh(\Gamma_2^4) \quad (12)$$

The mixing function (f_1) can be calculated using the following expression:

$$f_1 = \tanh(\Gamma_1^4) \quad (13)$$

The diffusivity efficiencies, Γ_2 and Γ_1, can be expressed by equations (14) and (15) as follows:

$$\Gamma_2 = \max\left(\frac{2\sqrt{k}}{0.09\omega d}, \frac{500\mu}{\omega d^2}\right) \quad (14)$$

$$\Gamma_1 = \min\left[\max\left(\frac{\sqrt{k}}{0.09\omega d}, \frac{500\mu}{\omega d^2}\right), \frac{4\rho\sigma_{\omega 2} k}{CD_{k\omega} d^2}\right] \quad (15)$$

Within the context of this equation, the variable d represents the distance to the wall that is closest to the subject, whereas CDkω represents the positive component of the cross-diffusion factor. It is possible to derive this term by using the equation that is presented in (16).

$$CD_{k\omega} = \max\left(2\rho\sigma_{\omega 2}\frac{1}{\omega}\frac{\partial k}{\partial x_j}\frac{\partial \omega}{\partial x_i}, 10^{-20}\right) \quad (16)$$

The calculation that is given below, which is based on the constants ϕ1 and ϕ2, is used to determine the constants ϕ that are represented in the new model.

$$\phi = f_1 \phi_1 + (1 - f_1)\phi_2 \quad (17)$$

The constants are expressed in the following manner: It is [46]:

$$\beta^* = 0.09,\ \phi_1 = \frac{5}{9},\ \beta_{1\backslash} = 0.075,\ \sigma_{k1} = 0.85,\ \sigma_{\omega 1} = 0.5$$

$$\phi_2 = 0.04, \beta_{2\backslash} = 0.0828, \sigma_{k2} = 1, \sigma_{\omega 2} = 0.856$$

An equation that may be used to calculate the Nusselt number is [47]:

$$Nu = \frac{hq}{\lambda(T_w - T_b)} \quad (18)$$

It is essential to take into consideration that in this equation, the symbols T_w and T_b indicate the local temperatures of the heated surface and the fluid, respectively. Additionally, the symbol q represents

the heat flow per unit area, while the symbols λ and h represent the fluid thermal conductivity and the convective heat transfer coefficient, respectively.

2.3. Grid generation and independence test

The mesh is important for the convergence of the simulations. A non-uniform grid was used, including increased density in regions of high gradient and low density elsewhere, to ensure that the computing effort was kept to a minimum while yet providing enough precision [48]. We chose a tetrahedral mesh because it can properly mimic complicated geometries, including lobed and swirling diffusers, and flow interactions in locations with significant velocity and temperature gradients. The mesh used in this work gives higher numerical stability and guarantees the correctness of results due to the better flexibility to complicated flow topologies. Due to the symmetry, just a quarter of the domain is evaluated to decrease the calculation time, as seen in figure 3. Four different mesh designs were built and tested for the optimal convergence behavior (Table 1). The fourth mesh with 4 712 552 elements was the most optimum in terms of convergence and lowest y+ value among the four meshes. This lower y+ is crucial to capture the near-wall turbulence correctly and to get more dependable findings. The improved mesh in important locations helped to increase the accuracy of solutions, while decreasing the computing costs. These results underline the necessity of mesh optimization in turbulence modeling.

Table 1. Grid independence tests

Mesh	Number of nodes	$\overline{y^+}$	$\overline{Nu}$
Mesh 1	204185	4.308	115.23
Mesh 2	424054	2.560	119.26
Mesh 3	515675	0.701	120.86
Mesh 4	845051	0.308	121.04

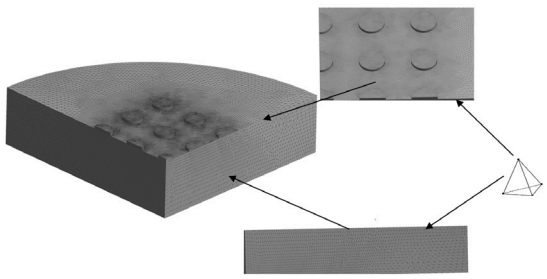

Figure 3. Meshing of the calculation domain

2.4. Boundary condition

To solve the pressure-velocity coupling, the Green-Gauss node-based gradient discretization was used in conjunction with the coupled solver software. To discretizing pressure, the PRESTO approach was used. This technique is particularly well-suited for the resolution of steep pressure gradients, such as those that are present in impinging and swirling jet environments. A second-order central difference scheme was used to discretize the diffusion terms that were included in the governing equations. and the convective components were discretized by a second-order upwind scheme. Both schemes were used to discretize the components.

Table 2. Simulation settings parameters and boundary conditions

Simulation type	3D steady
Turbulence model	SST k-ω
Convergence criterion	10^{-5}
Height	H = 80 mm
Reynolds number	Re = 11600
Diffuser diameter	D = 40 mm
Inlet	U = 5.27 $m.s^{-1}$, T = 300 K
outlet	P_{out}= 101325 Pa,
Dynamic Viscosity	$\mu = 1.8375*10^{-5}$ $kg.m^{-1}.s^{-1}$
Fluid density	$\rho = 1.225$ $kg.m^{-3}$
thermal conductivity	$\lambda = 0.0242$ $W.m^{-1}.K^{-1}$
Specific heat capacity at constant pressure	$Cp = 1006.43$ $J.kg^{-1}.K^{-1}$
Heat flux at the impingement surface	$q=1120$ $W.m^{-2}$
Turbulence intensity	I=5%

2.5. Validation with literature

To verify our model, we have compared the simulation results with the experimental and numerical data of the k-*ω* SST model, taken from the literature [8, 49-52] under the same circumstances. The axial velocity distribution for the single diffuser system is shown on figure 4. The simulation results show that the model is effective to solve the issue properly with the error margin of 8% at most. This difference may be due to numerous variables, such as the shape of the diffuser, intake velocity conditions, turbulence intensity, and others connected to the flow, that may be different between the simulated and experimental configurations. These error causes are typical in CFD simulations and are described extensively in literature [52–54]. The findings confirm that the model can match the actual flow characteristics.

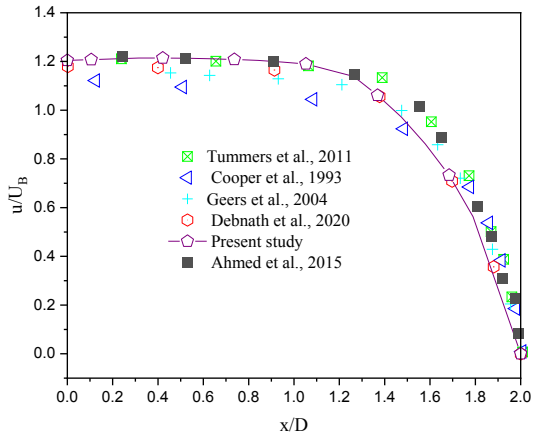

Figure 4. Axial velocity distribution of a single jet

3. Results

In this part, the results of the simulation for the air distribution system are shown. This section also includes a comprehensive analysis of dynamic and thermal properties.

3.1. Dynamic and thermal fields of the configuration 1 and 2

Figure 5 presents the velocity contours for both configurations at different axial stations along the flow direction. The velocity reaches its peak at the station next to the diffuser outlets, then diminishing as the distance from the outlet rises. This decrease continues until the station is located closest to the impact surface at x/D=1.9. Configuration 1 shows the most efficient mixing, with a more uniform velocity distribution across the flow field compared to the other configuration, indicating better turbulence and flow interaction.

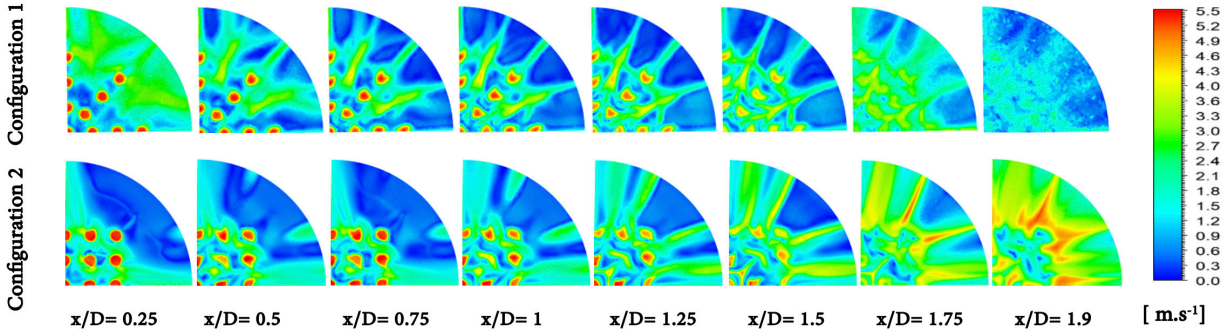

Figure 5. Velocity contours of the circular and square arrangement configurations

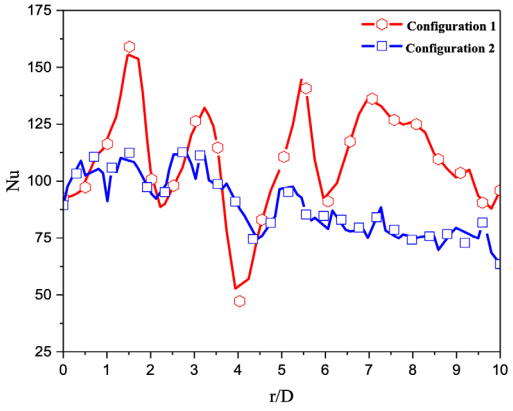

Figure 6. Nusselt number plotted on the y-axis, with x = 2D

3.2. Optimal configuration identification

Based on the previously obtained results, the circular configuration has proven its effectiveness in both dynamic and thermal aspects. Debnath et al.[8] have already demonstrated that, for a circular configuration, a staggered arrangement is the most suitable, which justifies this choice.

The distributions of the Nusselt number for the two configurations shown in figure 6 are representative of its fluctuation over the impact surface from the thermal point of view. For configuration 2, the Nusselt number exhibits a reasonably constant tendency with little variances around the mean, indicating stable and uniform heat transmission behavior. In contrast, configuration 1 exhibits stronger spatial changes of the Nusselt number, which suggests large volatility of the local heat transfer coefficients. Furthermore, despite these variations, the mean Nusselt number for Configuration 1 is higher than the other configurations, which indicates that the overall convective heat transfer efficiency is improved. The improvement is caused by the greater turbulence intensity and more efficient flow mixing of Configuration 1, which boosts the convective heat transfer rate at the surface.

The velocity contours for each configuration presented in figure 7, shown at various stations along the flow path, illustrate the distribution of velocity within the system. The velocity is maximum at the diffuser outputs, when the flow is completely formed, and declines steadily downstream until it is almost nil at the impact surface. This slow decay is governed by momentum diffusion and energy dissipation which are greatly impacted by the diffuser design. As for the tested configurations, the maximum velocity at the outflow is for the lobed diffuser. This is because of its unique shape which improves flow acceleration and decreases flow separation. The lobed shape helps to increase momentum transfer, which improves overall flow efficiency, helps to keep turbulence levels high and ensures better energy distribution throughout the system. As we move closer to the impact surface, starting from the station at x/D = 1.75, a marked increase in flow mixing is observed. This mixing is crucial as it contributes to a more uniform velocity distribution and helps to mitigate the adverse effects of flow stagnation. As a result of the greater mixing that occurs in the lobed diffuser arrangement, which plays a substantial part in increasing the overall performance, this configuration is preferred over the others.

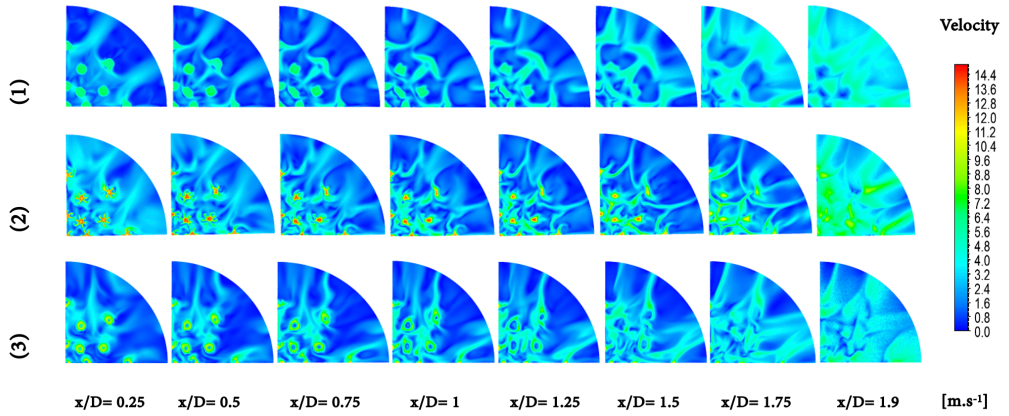

Figure 7. Velocity contours of the circular, lobed, and swirling diffuser configurations

In contrast to the velocity contours, the static pressure contours shown in figure 8 reveal a different distribution trend. At the diffuser exits, static pressure is at its lowest due to the acceleration of the flow, but it gradually increases as the flow decelerates while approaching the impact surface. The diffuser's center exhibits the maximum static pressure. The circular arrangement of diffusers leads to a somewhat homogeneous static pressure distribution with the maximum values in the vicinity of the diffuser outputs. This is most likely owing to the more traditional design that does not create major flow disruptions. In contrast, the lobed diffuser design yields the largest static pressure peak, which is ascribed to the higher flow deceleration produced by the lobed geometry. This design improves the pressure recovery due to the improved flow distribution within the diffuser. The swirling diffuser structure, however, is not the greatest in static pressure, but it is quite successful in inducing mixing of the flow. The swirling motion helps disperse the flow uniformly, which enhances the overall uniformity and reduces the possibility of flow separation at the impact surface. This trade-off between pressure recovery and flow mixing makes the swirling diffuser especially suitable in situations needing a high degree of flow homogeneity.

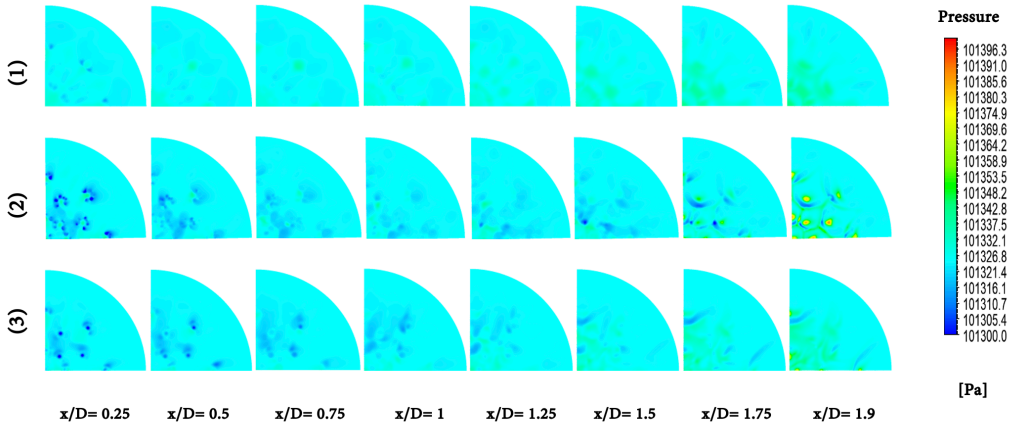

Figure 8. Contours of static pressure for the circular, lobed, and swirling diffuser configurations

The axial velocity distribution for the three diffuser designs is illustrated in figure 9, and the behavior of all configurations is shown. The velocity profile depends on the diffuser shape. Velocity rises to a maximum in both the lobed and circular forms and then decreases gradually as momentum is dissipated to eventually approach zero at the impact surface. On the other hand, the velocity distribution of the swirling diffuser is oscillatory, which is a sign of the recirculation zones created by the rotating flow. These recirculation zones promote greater flow spread and better mixing; so, the swirling diffuser is especially well suited for applications needing more uniform flow distribution. The lobed diffuser configuration has the maximum amplitude at their corresponding velocity peaks, roughly double the amplitude of the circular diffuser arrangement. This increased velocity at the peak can be attributed to the enhanced flow dynamics induced by the lobed geometry, which promotes better flow acceleration and reduces flow separation compared to the circular diffuser.

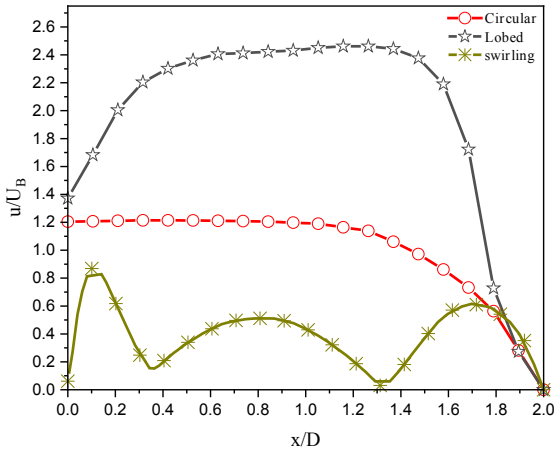

Figure 9. Axial velocity distribution of the circular, lobed, and swirling diffuser configurations

The radial velocity distribution for the three diffuser configurations is shown in figure 10. The distribution is characterized by non-uniform behavior, which is similar with the observations of [21], with distinct velocity peaks at the center of the diffuser, which decrease as the flow moves radially outward. Subsequently, the velocity gradually increases again as it approaches the diffuser's periphery. Velocity variations are caused by the presence of recirculation zones and the lack of a diffuser in the spacing area. These recirculation zones disrupt the smooth acceleration of the flow, leading to localized decreases in radial velocity. This phenomenon appears from the first diffuser center to the last, ranging from x/D = 0.25 to x/D = 1.50.

Beyond these stations, specifically from x/D = 1.75 to x/D = 1.90; i.e., close to the impact surface; the velocity shows a notable decrease, reaching almost zero at the central region of the diffuser for both the circular and lobed diffuser configurations. However, as the flow continues toward the impact surface, the velocity begins to recover, adopting a profile that mirrors the distribution seen at earlier stations, where velocity gradually increases toward the outer radius. This means that flow gradually stabilizes and tends towards a more uniform distribution in the periphery even while there are a high-pressure loss and flow slowing in the core region. The shape of the lobed diffuser results in the greatest velocity amplitudes and hence the best flow acceleration among the evaluated configurations. The lobes are useful in reducing flow separation and improving the diffusion process. This results in greater velocities at the diffuser exits. On the contrary, the swirling diffuser arrangement, while not the one delivering the greatest peak velocities, is the best in terms of flow spread. The swirling diffuser generates recirculation zones that enhance mixing, which is desirable for situations in which a uniform flow distribution is required. Finally, the circular diffuser arrangement provides the most stable radial velocity distribution with considerably smaller variations than the other two layouts. This stability is due to its more basic shape providing a more uniform flow profile but without the increased mixing or acceleration of the lobed and swirling diffusers.

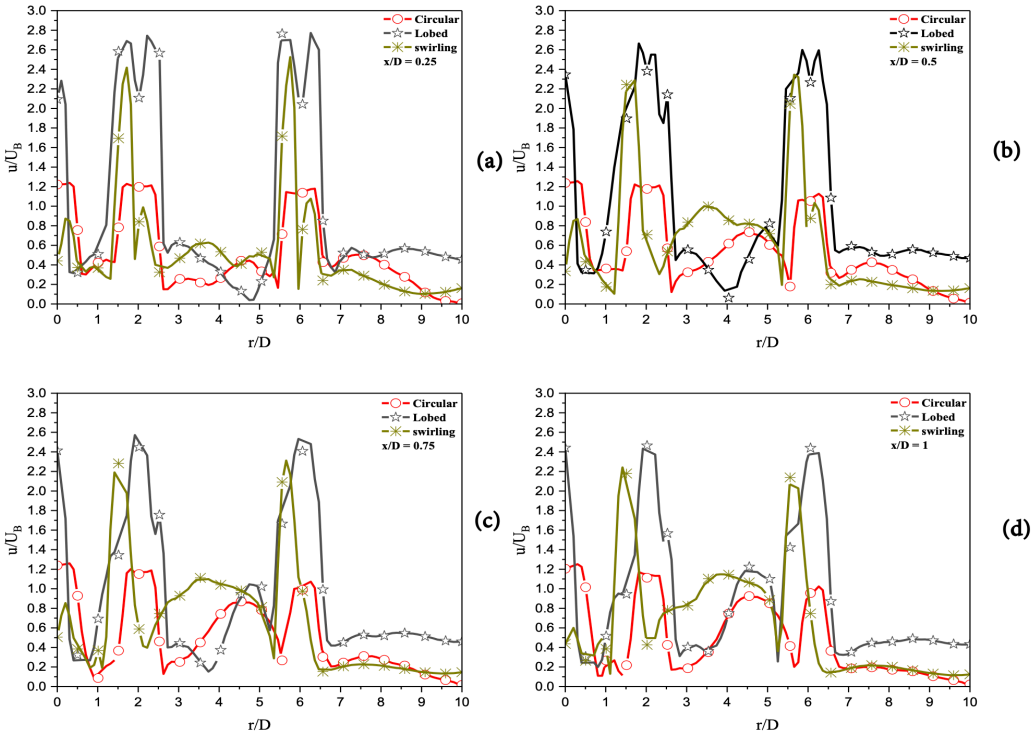

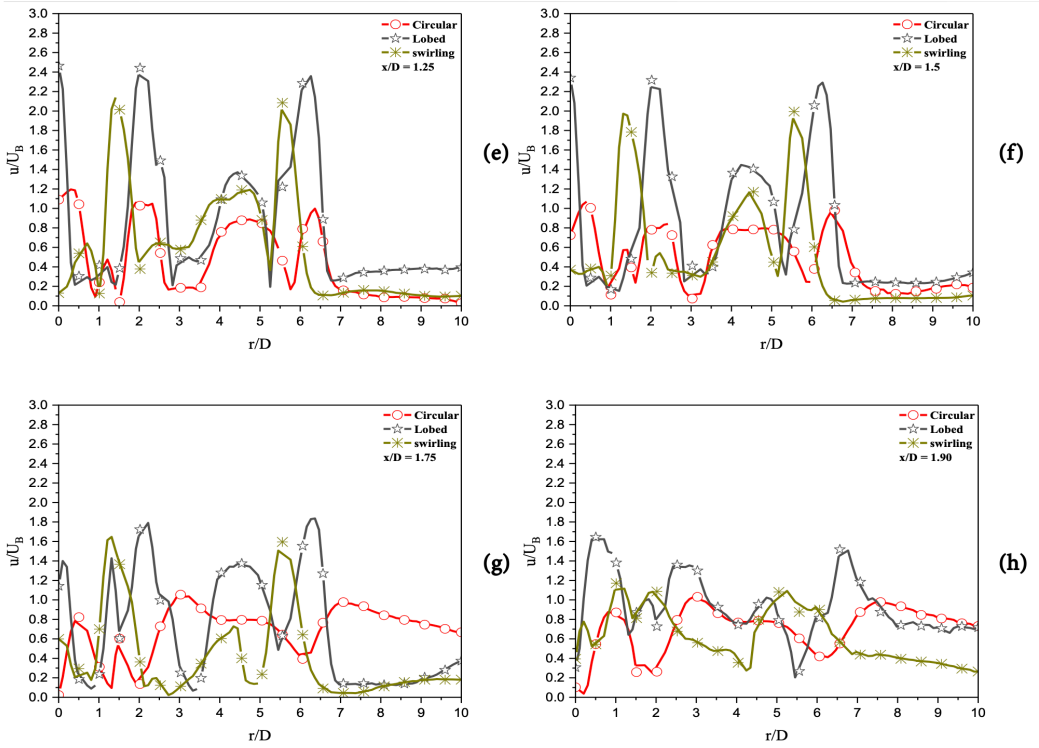

Figure 10. Radial velocity distribution of the circular, lobed, and swirling diffuser configurations

The contours of turbulent kinetic energy (k) at stations for each of the three configurations are shown in figure 11. Turbulent energy becomes significant starting at x/D = 1 and gradually decreases as the flow approaches the impact surface. Increased shear and vortex formation are projected to give rise to strong turbulence throughout the circle of the air jet, with the strongest turbulence being in the lobed jet shape. The swirling jet shape likewise produces considerable turbulence as found by Debnath et al. [8], although significantly less than that of the lobed jet owing to the rotating flow. On the other hand, the circular jet design shows the minimum turbulent kinetic energy values since it has a more uniform flow profile, which results in less turbulence and a more stable jet. This lower turbulence may be advantageous in applications requiring less flow instability, but it also limits mixing and spread.

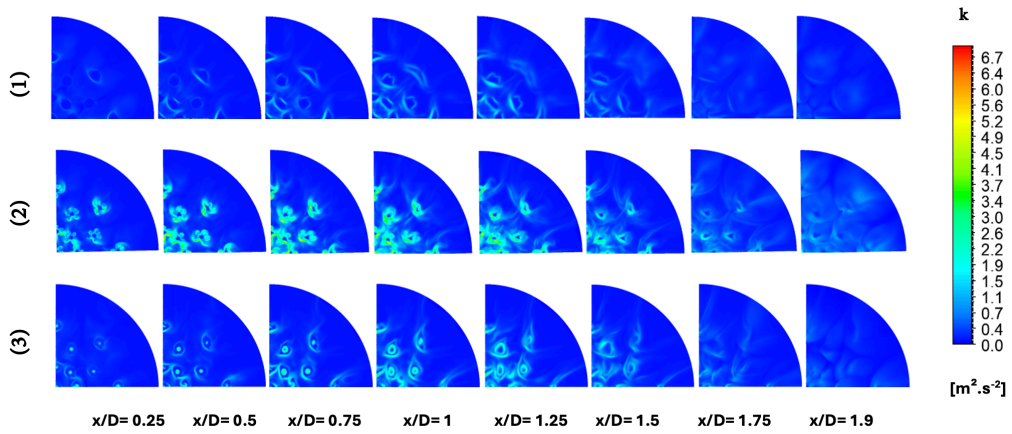

Figure 11. Contours of turbulent kinetic energy for the circular, lobed, and swirling diffuser configurations

Figure 12. shows the contour of the convective heat transfer coefficient at the surface. This parameter quantifies the efficiency of heat exchange between the surface and the flow, directly reflecting the convective heat transfer capability of the system. An important aspect of the convective heat transfer coefficient is its relationship to the conveyance of thermal energy, which is heavily impacted by

the flow behavior, the turbulence intensity and the diffuser shape. The lobed jet arrangement has the greatest convective heat transfer coefficient of the three arrangements, indicating that it leads to superior heat transfer efficiency. The coefficient rises near the periphery of the diffuser where turbulent flow increases mixing and heat transmission. The heat transfer coefficient decreases with increasing distance from diffusers, demonstrating that the diffuser shape has a decreasing influence on convective exchange. This trend is seen for all designs. However, the lobed jet configuration has a higher overall coefficient indicating its better heat transfer capability.

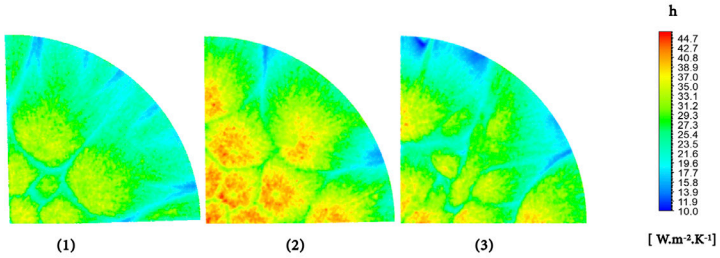

Figure 12. Contours of the convection coefficient for the circular, lobed, and swirling diffuser configurations at the impact surface

The figure 13 shows the Nusselt number (Nu) distribution for the three jet configurations that impact along the radial line. The results show that the Nu profile on the impact surface is radially non-uniform, which is similar with the observations of Geers et al. [50] impinging normally on a plane wall, using particle image velocimetry (PIV and Draksler et al. [55]. The maximum Nusselt number occurs at the wall of each diffuser and decays till the next diffuser. This pattern continues until about r/D=7 when a little variance in Nu is seen, which is most likely owing to the lack of a diffuser in this area. Out of all the configurations the lobed diffuser has the greatest Nusselt number i.e. most effective heat transmission at the surface. Following this is the whirling diffuser, which also allows for quite significant heat transmission but not as much as the lobed design. The circular diffuser arrangement, while characterized by lower Nusselt numbers than the other two, retains a reasonable degree of stability throughout the radial profile, with less variance in heat transfer efficiency. This stability may be advantageous in applications requiring consistent thermal performance. The axial temperature distribution presented in the figure 14 remains relatively stable from the diffuser outlets up to station x/D = 1.25. Beyond this point, the swirling diffuser configuration begins to show an increase in temperature, which continues until it reaches the impact surface. For the other two configurations, the temperature increases start at later stations: x/D = 1.7 for the circular diffuser and x/D = 1.9 for the lobed diffuser. The increase in temperature across all configurations is mostly due to the thermal exchange between the heated impact surface and the surrounding air jet, which absorbs heat from the surface and elevates its temperature. There are changes in the flow dynamics and heat transfer characteristics for each configuration, which may be attributed to the delay in the temperature increase that occurs for both the circular and lobed diffusers.

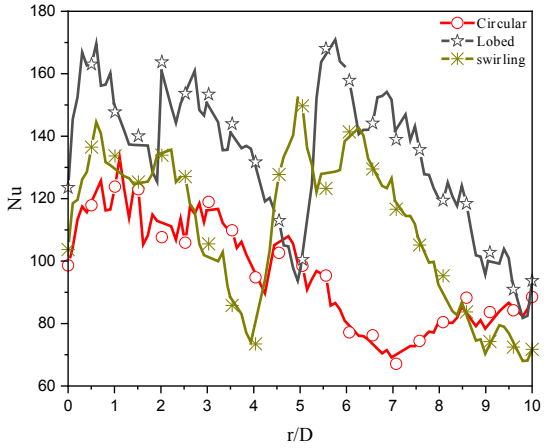

Figure 13. Nusselt number at the impact surface of circular, lobed, and swirling diffuser configurations along the radial direction

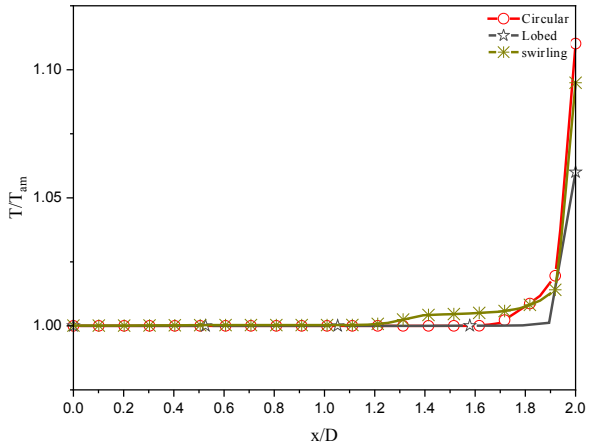

Figure 14. Axial temperature distribution of circular, lobed, and swirling diffuser configurations

The radial temperature distribution at different locations along the flow route is shown in figure 15, which shows the temperature evolution when the flow interacts with the heated surface. The temperature amplitude grows with the flow approaching the impact surface, which indicates a convective heat exchange between the hot plate and the ambient air jet. The first four stations in the middle of the diffuser are at low temperatures, suggesting restricted heat transmission. However, as the flow passes the first diffuser, the temperature begins to increase, indicating the growing heat absorption by the air jet. The temperature keeps on increasing until it reaches its maximum in the area where the diffuser is offset and then it starts decreasing as the flow moves downstream.

In terms of diffuser designs, the swirling diffuser exhibits a significant improvement in temperature at later stations, exceeding the lobed diffuser, which had the maximum temperatures between x/D = 1.25 and x/D = 1.50 originally. The increased heat transfer in the swirling diffuser may be ascribed to the generated vortex structures and improved mixing which facilitates the heat transfer between the

surface and the flow more efficiently. Previously the lobed diffuser had greater temperatures. As the whirling design becomes more efficient, the lobed diffuser begins to fall. The results at the last two stations show that the circular diffuser design has the lowest temperature rise, which indicates a more stable but less effective heat transfer mechanism than the other two layouts. This consistency might be helpful in situations that need more.

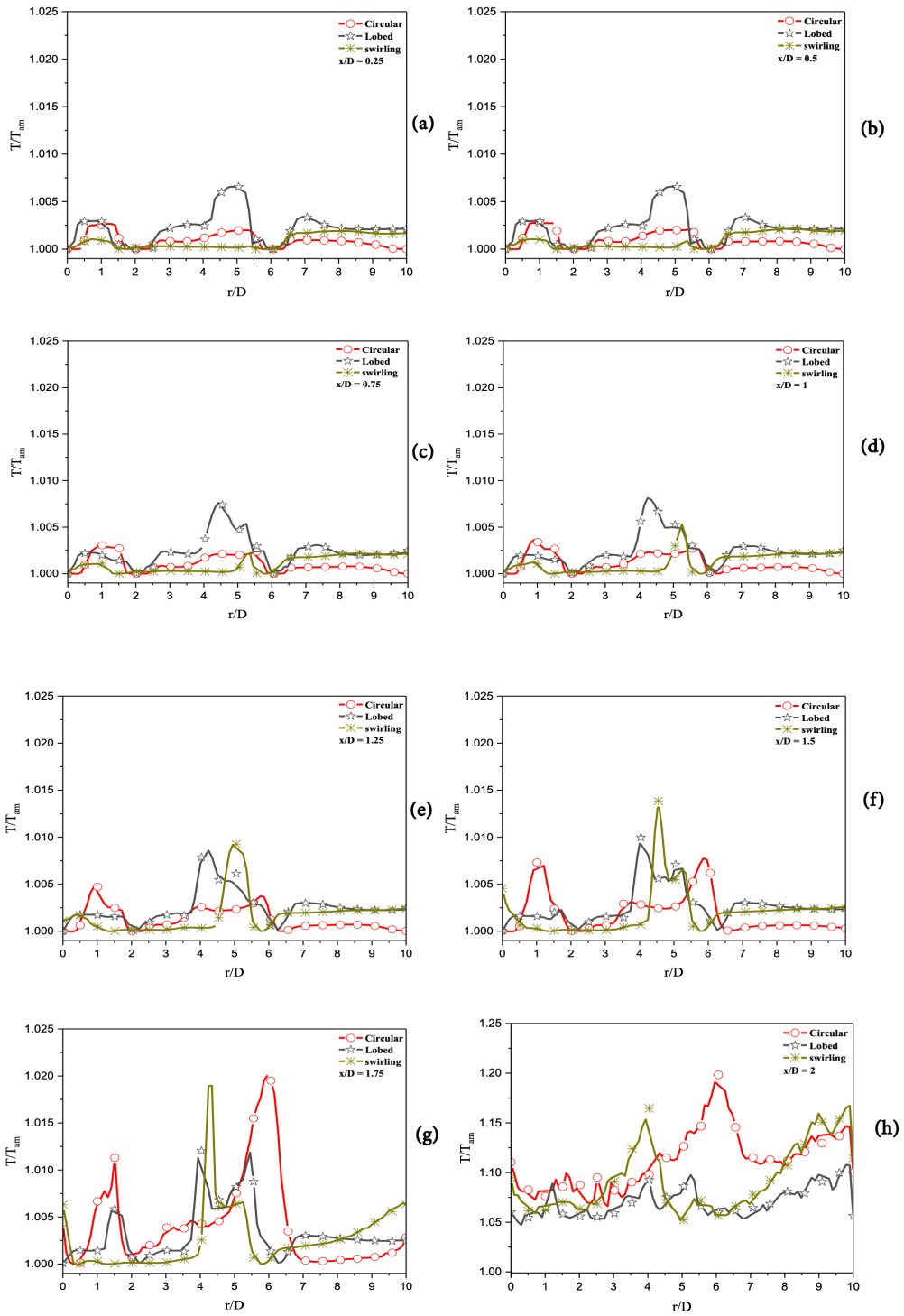

Figure 15. Radial temperature distribution of the circular, lobed, and swirling diffuser configurations

4. Conclusion

According to the results of the numerical simulations conducted using the SST k-ω turbulence model, the diffuser shape has a considerable effect on air distribution and impinging jet heat transfer efficiency. An unique technique in the realm of impinging jet cooling is provided by comparing the properties of three air diffusion systems with numerous jets impinging on a hot plate. The findings demonstrate that the SST k-ω model predicts dynamic and thermal properties rather correctly with a maximum error of 8% which agrees well with experimental data. The shape and layout of the diffuser are of great importance for the thermal and dynamic performance of the system. The major results of the research are as follows:

- Configuration 1 augments convective heat transfer by facilitating enhanced mixing and greater turbulence, hence yielding a larger average Nusselt number. Nonetheless, this results in diminished stability relative to other setups. Configuration 2 offers greater stability but exhibits lower thermal efficiency due to less pronounced fluctuations in heat transfer.
- The lobed diffuser generates the highest outlet velocities, reduces flow separation, and enhances jet acceleration. This configuration leads to a 31.7% improvement in thermal transfer compared to the circular diffuser, promoting better mixing and more uniform velocity distribution.
- The swirling diffuser excels in promoting flow mixing, creating recirculation zones that improve flow uniformity. Although its thermal performance is slightly lower than that of the lobed diffuser, it still demonstrates a 16.26% improvement in thermal transfer relative to the circular diffuser.
- The circular diffuser, characterized by its simple shape, offers enhanced jet stability but exhibits lower efficiency in flow acceleration and heat transmission, making it less effective than other diffuser geometries.

In summary, the lobed diffuser offers the optimal balance of flow acceleration, reduced separation, and improved thermal performance.

Nomenclature

C_p	specific heat capacity [$j.kg^{-1}.K^{-1}$]
d	Diameter of the plate surface[m]
D	Diffuser diameter [m]
H	Nozzle to plate distance (2D) [m]
h	Surface heat transfer coefficient [$W.m^{-2}.K^{-1}$]
k	Turbulent kinetic energy [$m^2.s^{-2}$]
Nu	Nusselt number [dimensionless]
r	Radial co-ordinate [m]
Re	Reynolds number [dimensionless]
S	Swirl number
u	Mean velocity [$m.s^{-1}$]
U_B	Bulk axial velocity [$m.s^{-1}$]
x	Axial coordinate [m]
y, z	Cartesian coordinates [m]
ω	Specific turbulence dissipation rate [s^{-1}]
λ	thermal conductivity [$W.m^{-1}.K^{-1}$]
μ	Dynamic viscosity [$kg.m^{-1}.s^{-1}$]
μ_t	Turbulent dynamic viscosity [$kg.m^{-1}.s^{-1}$]

Acknowledgements

LCTMMS's head offered the laboratory needed for the study.

Conflict of interest

The authors of this study state that there are no conflicts of interest that are associated with the research, authorship, or publication of this manuscript under consideration.

Authors contribution

A.M. Maiga, and A. Khelil: Conceptualization, Investigation, reviewing, writing original draft, Editingand Supervision; M. Braikia: Conceptualization, Analysis, Visualization;A. FellagueChebra: Analysis and Reviewing.

References

[1] Han B, Goldstein RJ. Jet-impingement heat transfer in gas turbine systems. In Annals of the New York Academy of Sciences 2001;934: 147–161. https://doi.org/10.1111/j.1749-6632.2001.tb05849.x

[2] SARKAR A, NITIN N, KARWE MV, SINGH RP. Fluid Flow and Heat Transfer in Air Jet. Journal of Food Science Crh1132004;69(4): 113–122. https://doi.org/10.1111/j.1365-2621.2004.tb06315.x

[3] Bedrouni M, Khelil A, Braikia M, Naji H. Large eddy simulation of a turbulent flow over circular and mixed staggered tubes' cluster. Journal of Applied Fluid Mechanics 2020; 13(5):1471–1486. https://doi.org/10.36884/JAFM.13.05.31119

[4] Viskanta R . Nusselt-Reynolds Prize Paper Heat Transfer to Impinging Isothermal Gas and Flame Jets. Experimental Thermal and Fluid Science 1993; 6: 111–134. https://doi.org/10.1016/0894-1777(93)90022-B

[5] Rajak U, Nashine P, Chaurasiya PK, Verma TN. A numerical investigation of the species transport approach for modeling of gaseous combustion. Journal of Thermal Engineering 2021; 7: 1921–1935. https://doi.org/10.14744/jten.2021.0006

[6] Rajak U, Nashine P, Chaurasiya PK, Verma TN, Patel DK, DwivediG. Experimental & predicative analysis of engine characteristics of various biodiesels. Fuel 2021; 285:90-97. https://doi.org/https://doi.org/10.1016/j.fuel.2020.119097

[7] Behnia M, Parneix S, Durbin P. Accurate modeling of impinging jet heat transfer. Center Turbulence Research Annual Research Briefs 1997;0: 149–164. http://ctr.stanford.edu/ResBriefs97/behnia.pdf

[8] Debnath S, Khan MHU, Ahmed ZU. Turbulent swirling impinging jet arrays: A numerical study on fluid flow and heat transfer. Thermal Science and Engineering Progress 2020;19. https://doi.org/10.1016/j.tsep.2020.100580

[9] Geers LFG, Hanjalić K, Tummers MJ. Wall imprint of turbulent structures and heat transfer in multiple impinging jet arrays. Journal of Fluid Mechanics 2006; 546: 255–284. https://doi.org/10.1017/S002211200500710X

[10] Weigand B, Spring S. Multiple jet impingement. A review. Heat Transfer Research 2011;42(2): 101–142. https://doi.org/10.1615/HeatTransRes.v42.i2.30

[11] Giorges ATG, Forney LJ, Wang X. Numerical study of multi-jet mixing. Chemical Engineering Research and Design 2001;79(5): 515–522. https://doi.org/10.1205/02638760152424280

[12] Braikia M, Loukarfi L, Khelil A, Naji H. Improvement of thermal homogenization using multiple swirling jets. Thermal Science 2012; 16(1): 239–250. https://doi.org/10.2298/TSCI101026131B

[13] Roudane M, Loukarfi L, Khelil A, Hemis M. Numerical investigation of thermal characteristics of confined rotating multi-jet. Mechanics and Industry 2013; 14(4):317–324. https://doi.org/10.1051/meca/2013071

[14] Bennia A, Loukarfi L, Khelil A, Mohamadi S, Braikia M, Naji H. Contribution to the experimental and numerical dynamic study of a turbulent jet issued from lobed diffuser. Journal of Applied Fluid Mechanics 2016; 9(6): 2957–2967. https://doi.org/10.29252/jafm.09.06.25953

[15] Aziz MA, Gad IAM, Mohammed ESFA, Mohammed RH. Experimental and numerical study of influence of air ceiling diffusers on room air flow characteristics. Energy and Buildings 2012; 55: 738–746. https://doi.org/10.1016/j.enbuild.2012.09.027

[16] Meslem A, Dia A, Beghein C, El M, Nastase I, Vialle P. A comparison of three turbulence models for the prediction of parallel lobed jets in perforated panel optimi z ation. Building and Environment 2011; 46(11): 2203–2219. https://doi.org/10.1016/j.buildenv.2011.04.037

[17] Suzuki T, Tsujimoto K, Shakouchi T, Ando T. DNS of flow and heat transfer characteristics of multiple impinging jets. Proceedings of the 21st Australasian Fluid Mechanics Conference, AFMC 2018; 6–9. https://doi.org/10.1299/jsmemecj.2018.s0510502

[18] Gupta AK, Lilley DG, Syred N. Book Review. Combustion and Flame 1986; 63, 311. http://dx.doi.org/10.1016/0010-2180(86)90133-1

[19] Wigley G, Clark JA. Heat transport coefficients for constant energy flux models of broad leaves. Boundary-Layer Meteorology 1974;7(2):139–150. https://doi.org/10.1007/BF00227909

[20] Vamsi BVRS, RAVEENDIRAN P, SASTRY MRC. Experimental and numerical study of fluid flow and heat transfer in the impinging of inline round jets. Journal of Thermal Engineering 2025; 11(1): 270–289. https://doi.org/10.14744/thermal.0000918

[21] Medaouar W, Loukarfi L, Braikia M, Khelil A, Naji H. Experimental and Numerical Study of a Turbulent Multiple Jets Issued from Lobed Diffusers. Journal of Applied Fluid Mechanics 2019; 12(3): 729–742. https://doi.org/10.29252/jafm.12.03.29476

[22] Chebra AF, Braikia M, Khelil A, Bedrouni M, Zied D. Numerical study of turbulent flows around a cubic obstacle blown from a variable geometry jets diffuser. Ecosistemas 2024; 18(1):25–54. https://doi.org/10.24132/acm.2024.837

[23] Zahout N, Braikia M, Khelil A, Naji H. Thermal and dynamic characterization of a multi-jet system with different geometry diffusers. Journal of Thermal Engineering2024;10(2): 404–429. https://doi.org/10.18186/thermal.1456643

[24] Ghalem M, Zahaf S, Dahmane M, Atmane HA, Bennai R. (2025). Natural frequencies of 2D-FG beams with internal crack defects on Winkler–Pasternak elastic foundation using finite element technique. Mechanics Based Design of Structures and Machines; 2025:1-18. https://doi.org/10.1080/15397734.2025.2458097

[25] Benkhettab M, Dahmane M, Zahaf S, Ait Atmane H, Bennai R, Hadji L, Madan R. Computational study on linear vibration and thermal buckling of fluid-conveying pipes. Advances in Concrete Construction 2025; 19(2): 93–100. https://doi.org/https://doi.org/10.12989/acc.2025.19.2.093

[26] Zahaf S, Dahmane M, Belaziz A, Bouri I, Afane N. Failure Analysis of Semi-Elliptical Crack Behavior in the Cement Mantle of a Total Hip Prosthesis. Materials Physics and Mechanics 2022; 48(2): 242–271. https://doi.org/10.18149/MPM.4822022_9

[27] Rajak U, Nashine P, Verma T. N. Comparative Assessment of The Emission Characteristics of First, Second and Third Generation Biodiesels As Fuel in A Diesel Engine. Journal of Thermal Engineering 2020;6(6): 211–225. https://doi.org/10.18186/THERMAL.818036

[28] [28]Rajak U, Panchal M, Viswanath Allamraju K, Nashine P, Nath Verma T, Pugazhendhi A. A numerical investigation on a diesel engine characteristic fuelled using 3D CFD approach. Fuel 2024;368: 131488. https://doi.org/https://doi.org/10.1016/j.fuel.2024.131488

[29] Zerrout A, Khelil A, Loukarfi L. Heat Transfer of Swirling Multi Jets Impinging System. Journal of Mechanical Engineering 2020; 17(2): 93–108. https://doi.org/10.24191/jmeche.v17i2.15303

[30] Dahmane M, Boutchicha D, Adjlout L. One-way fluid structure interaction of pipe under flow with different boundary conditions. Mechanika 2016; 22(6): 495–503. https://doi.org/10.5755/j01.mech.22.6.13189

[31] Goodarzi M, Safaei MR, Vafai K, Ahmadi G, Dahari M, Kazi SN, Jomhari N. Investigation of nanofluid mixed convection in a shallow cavity using a two-phase mixture model. International Journal of Thermal Sciences 2014; 75: 204–220. https://doi.org/10.1016/j.ijthermalsci.2013.08.003

[32] Khelil A, Naji H, Loukarfi L, Meliani MH, Braikia M. (2016). Numerical simulation of the interactions among multiple turbulent swirling jets mounted in unbalanced positions. Applied Mathematical Modelling 2016; 40:3749–3763. https://doi.org/10.1016/j.apm.2015.10.047

[33] Bahmani MH, Sheikhzadeh G, Zarringhalam M, Akbari OA, Alrashed AAAA, Shabani GAS, Goodarzi, M. Investigation of turbulent heat transfer and nanofluid flow in a double pipe heat exchanger. Advanced Powder Technology 2018; 29(2): 273–282. https://doi.org/10.1016/j.apt.2017.11.013

[34] Koseoglu MF, Baskaya S. The effect of flow field and turbulence on heat transfer characteristics of confined circular and elliptic impinging jets. International Journal of Thermal Sciences 2008; 47(10): 1332–1346. https://doi.org/10.1016/j.ijthermalsci.2007.10.015

[35] Tatsumi K, Tanaka M, Woodfield PL, Nakabe K. (2010). Swirl and buoyancy effects on mixing performance of baffle-plate-type miniature confined multijet. International Journal of Heat and Fluid Flow 2010; 31(1): 45–56. https://doi.org/10.1016/j.ijheatfluidflow.2009.09.005

[36] Choi SK, Kim SO. Turbulence modeling of natural convection in enclosures: A review. Journal of Mechanical Science and Technology 2012, 26(1): 283–297. https://doi.org/10.1007/s12206-011-1037-0

[37] Prasad KSR, Krishna V, Bharadwaj S. Effect of heat flux and mass flux on the heat transfer characteristics of supercritical carbon dioxide for a vertically downward flow using computational fluid dynamics and artificial neural networks. Journal of Thermal Engineering 2023; 9(5): 1291–1306. https://doi.org/10.18186/thermal.1376850

[38] Wilcox DC. Reassessment of the scale-determining equation for advanced turbulence models. AIAA Journal 1988;26(11): 1299–1310. https://doi.org/10.2514/3.10041

[39] Podila K, RaoY. CFD modelling of supercritical water flow and heat transfer in a 2 × 2 fuel rod bundle. Nuclear Engineering and Design 2016; 301: 279–289. https://doi.org/10.1016/j.nucengdes.2016.03.019

[40] Menter FR. Two-equation eddy-viscosity turbulence models for engineering applications. AIAA Journal 1994; 32(8): 1598–1605. https://doi.org/10.2514/3.12149

[41] Safaei MR, Togun H, Vafai K, Kazi SN, Badarudin A. Investigation of heat transfer enhancement in a forward-facing contracting channel using FMWCNT nanofluids. Numerical Heat Transfer; Part A: Applications 2014; 66(12): 1321–1340. https://doi.org/10.1080/10407782.2014.916101

[42] Togun H, Safaei MR, Sadri R, Kazi SN, Badarudin A, Hooman K, Sadeghinezhad E. Numerical simulation of laminar to turbulent nanofluid flow and heat transfer over a backward-facing step. Applied Mathematics and Computation 2014; 239: 153–170. https://doi.org/10.1016/j.amc.2014.04.051

[43] Huang H, Sun T, Zhang G, Sun L, Zong Z. Modeling and computation of turbulent slot jet impingement heat transfer using RANS method with special emphasis on the developed SST turbulence model. International Journal of Heat and Mass Transfer 2018; 126: 589–602. https://doi.org/10.1016/j.ijheatmasstransfer.2018.05.121

[44] Huang H, Sun T, Zhang G, Li D, Wei H. Evaluation of a developed SST k-Ω turbulence model for the prediction of turbulent slot jet impingement heat transfer. International Journal of Heat and Mass Transfer 2019;139:700–712. https://doi.org/10.1016/j.ijheatmasstransfer.2019.05.058

[45] Ahmadi Nadooshan A, Mohammadi S, Bayareh M. Heat Transfer and Friction Characteristics of an Array of Perforated Fins Under Laminar Forced Convection. Journal of Thermal Engineering 2019; 5(3): 115–122. https://doi.org/10.18186/THERMAL.540007

[46] Chebra AF, Khelil A, Braikia M, Bedrouni M. Comparative analysis of modified jet diffuser geometry for evaluating the impact of rounded edges and chamfered design on cooling efficiency of electronic components in cross flow and impinging jet. Journal of Thermal Engineering 2024; 10(4): 961–977. https://doi.org/10.14744/thermal.0000849

[47] Rana S, Dura HB, Bhattrai S, Shrestha R. Impact of baffle on forced convection heat transfer of CuO/water nanofluid in a micro-scale backward facing step channel. Journal of Thermal Engineering2022; 8(3): 310–322. https://doi.org/10.18186/THERMAL.1107168

[48] Khelil A, Naji H, Braikia M, Loukarfi L. Comparative investigation on heated swirling jets using experimental and numerical computations. Heat Transfer Engineering 2015; 36(1): 43–57. https://doi.org/10.1080/01457632.2014.906279

[49] Cooper D, Jackson DC, Launder BE, Liao GX. Impinging jet studies for turbulence model assessment-I. Flow-field experiments. International Journal of Heat and Mass Transfer1993; 36(10):2675–2684. https://doi.org/10.1016/S0017-9310(05)80204-2

[50] Geers LFG, Tummers MJ, Hanjalić K. (2004). Experimental investigation of impinging jet arrays. Experiments in Fluids 2004; 36(6): 946–958. https://doi.org/10.1007/s00348-004-0778-2

[51] Tummers MJ, Jacobse J, Voorbrood, SGJ. Turbulent flow in the near field of a round impinging jet. International Journal of Heat and Mass Transfer 2011; 54:4939–4948. https://doi.org/10.1016/j.ijheatmasstransfer.2011.07.007

[52] Ahmed ZU, Al-Abdeli YM, Matthews MT. The effect of inflow conditions on the development of non-swirling versus swirling impinging turbulent jets. Computers and Fluids2015;118:255–273. https://doi.org/10.1016/j.compfluid.2015.06.024

[53] [53]Trinh XT, Fénot M, Dorignac E. The effect of nozzle geometry on local convective heat transfer to unconfined impinging air jets. Experimental Thermal and Fluid Science 2016; 70: 1–16. https://doi.org/10.1016/j.expthermflusci.2015.08.006

[54] Ikhlaq M, Al-Abdeli YM, Khiadani M. Nozzle exit conditions and the heat transfer in non-swirling and weakly swirling turbulent impinging jets. Heat and Mass Transfer/Waerme-Und Stoffuebertragung 2020; 56(1): 269–290. https://doi.org/10.1007/s00231-019-02710-1

[55] Draksler M, Končar B, Cizelj L, Ničeno B. Large Eddy Simulation of multiple impinging jets in hexagonal configuration – Flow dynamics and heat transfer characteristics. International Journal of Heat and Mass Transfer 2017; 109:16–27. https://doi.org/10.1016/j.ijheatmasstransfer.2017.01.080